Journal of the European Ceramic Society 42 (2022) 3004–3014

Contents lists available at ScienceDirect

Journal of the European Ceramic Society

journal homepage: www.elsevier.com/locate/jeurceramsoc

Hydrothermal synthesis and spark plasma sintering of NaY zeolite as solid-state matrices for cesium-137 immobilization

O.O. Shichalin [a,*], E.K. Papynov [a], V.A. Nepomnyushchaya [a], A.I. Ivanets [b], A.A. Belov [a], A. N. Dran'kov [a], S.B. Yarusova [c], I.Yu. Buravlev [a], A.E. Tarabanova [a], A.N. Fedorets [a], S.A. Azon [a], Z. E. Kornakova [a], S.Yu. Budnitskiy [d], I.G. Tananaev [a,e], Yun Shi [f,g], Yifei Xiong [f,h], Haibo Wang [h]

[a] *Far Eastern Federal University, 10 Ajax Bay, Russky Island, 690922 Vladivostok, Russia*
[b] *Institute of General and Inorganic Chemistry of National Academy of Sciences of Belarus, Surganova st. 9/1, Minsk 220072, Belarus*
[c] *Vladivostok State University of Economics and Service, Gogolya st., 41, Vladivostok 690014, Russia*
[d] *Far East Geological Institute, Far Eastern Branch of Russian Academy of Sciences, 159, Prosp. 100-letiya Vladivostoka, Vladivostok 690022, Russia*
[e] *Vernadsky Institute of Geochemistry and Analytical Chemistry of Russian Academy of Sciences, 19 Kosygin St., 119991 Moscow, Russia*
[f] *State Key Laboratory of High Performance Ceramics and Superfine Microstructure, Shanghai Institute of Ceramics, Chinese Academy of Sciences, Shanghai 200050, China*
[g] *Center of Materials Science and Optoelectronics Engineering, University of Chinese Academy of Science, Beijing 100049, China*
[h] *College of Material Science and Engineering, Nanjing Tech University, Nanjing 211816, China*

A R T I C L E I N F O

Keywords:
Ceramics
Aluminosilicates
Sorbents
Cesium
Radionuclides, Leaching Rate
Hydrolytic stability
Sintering
SPS

A B S T R A C T

Hydrothermal synthesis of NaY-type zeolite was carried out and the effect of temperature on the phase composition, crystal structure, textural characteristics, particle size and morphology, as well as sorption properties to Cs^+ ions was studied. Solid-state matrices based on NaY zeolite the Faujasite structure containing 26.1 wt% cesium were obtained by spark plasma sintering (SPS) with high values of compressive strength (to 132.9 MPa) and Vickers microhardness to HV~ 698, Fracture toughness (K_{1c}) ~ 1.26 MPa m$^{1/2}$. The kinetics of ceramic matrices consolidation, phase composition and morphology using dilatometric studies, XRD, and SEM were studied. The thermogravimetric analysis shown the high thermal stability of the obtained samples up to 1300 °C. The high hydrolytic stability of $CsAlSiO_4$ ceramic was proven (leaching rate of 2.33 $\times 10^{-8}$ g·cm^{-2}·day^{-1} and cesium diffusion coefficient De 1.41 $\times 10^{-13}$), which exceeds the requirements of GOST R 50926–96 and ISO 6961:1982 for solid-state matrices.

1. Introduction

The safety of the development of nuclear energy directly depends on solving the problem of handling and processing of radioactive waste. Many studies are aimed at studying various approaches to the management of spent nuclear fuel [1–7]. One of the concepts is the reuse of highly active waste, in particular ^{137}Cs, in ionizing radiation sources [8]. The danger of cesium radioactive isotopes for living organisms is associated with the solubility of most of its compounds and the high rate of migration in the environment. Therefore, in order to ensure the safe use of autonomous closed sources and prevent environmental pollution, it is necessary to use materials in which cesium is immobilized into solid-state mechanically strong matrices.

For the cesium isotopes immobilization as a highly active radioactive waste, glass and ceramic matrices of various compositions are used. Ceramics are characterized by higher physicochemical parameters than glass, in particular, compositions based on titanates, phosphates, aluminosilicates can be distinguished [9–22]. The advantage of aluminosilicates, as a class of inorganic polymers, is the ability to form layered and skeleton crystal structures, which causes their high specific surface area and correlates with the ion exchange capacity. Zeolites are a cheap and affordable material for obtaining solid-state matrices based on aluminosilicate ceramics.

The crystal structure of zeolites has two important features. Firstly, the aluminosilicate framework forms cavities, pores and channels in which molecules of only a certain size can be placed. Due to this, zeolites are capable of selective sorption by the molecular sieve mechanism and are highly selective sorbents. Secondly, the charge of AlO_4 and SiO_4

* Corresponding author.
E-mail address: oleg_shich@mail.ru (O.O. Shichalin).

https://doi.org/10.1016/j.jeurceramsoc.2022.02.007
Received 31 December 2021; Received in revised form 1 February 2022; Accepted 2 February 2022
Available online 4 February 2022

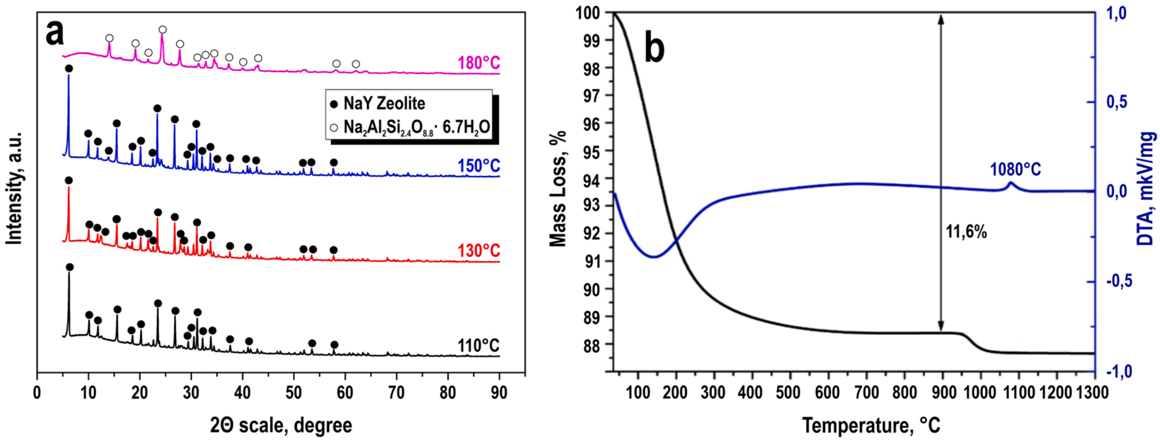

Fig. 1. (a) XRD patterns of zeolite samples and (b) DTA-TG curves of zeolite sample obtained at 110 °C after Cs+ ions saturation.

Table 1
Characteristics of NaY zeolite samples.

Temperature of synthesis, °C	Content of Cs^+ ions, wt % (AAS)	Content of Cs^+ ions, wt % (EDX)	$A_{BET\,sp}$, m^2/g	V_{HK}, cm^3/g	D_{HK}, nm
110	22.1	22.0	410	0151	0.43
130	26.1	25.9	417	0.153	0.43
150	21.5	20.7	620	0.224	0.43
180	3.0	2.0	13.6	0.009	0.54

tetrahedra is compensated by cations that are located in these voids and are capable of substitution by the mechanism of ion exchange. Therefore, the structure of the aluminosilicate frame is extremely resistant to radioactive radiation. These advantages make zeolites one of the most promising materials for cesium ions removal and immobilization. Thus, zeolites containing an 8-membered ring (8MR), such as mordenite, shabazite, LTE, show high selectivity for Cs^+. This selective coordination is explained by the comparable diameters of Cs^+ ions (3.6 Å) and the ring cavity (3.6–4.1 Å) [23,24].

Meanwhile, the use of synthetic zeolites has a number of advantages over natural ones, of which the main ones are consistency of composition, predictability of thermal behavior, absence of undesirable impurities, homogeneity of structure and reproducibility of physicochemical properties. Natural zeolite rocks contain zeolite in the range of 20–70 wt % and impurities of various cations, such as Na, K, Ca, Mg, Zn, Fe. During subsequent heat treatment, the zeolite containing cesium cations is able to reliably immobilize the radionuclide due to phase transformation into a denser monolithic nonporous structure, for example, pollucite. Since cesium chloride is able to volatilize when heated, sintering should be carried out at the lowest possible temperature and in the shortest time. Various sintering methods are successfully used to obtain materials based on zeolites that immobilize radionuclides [25–33]. One of the promising processing methods is spark plasma sintering, which makes it possible to obtain materials with high performance characteristics. This technology avoids the temperature gradient, significantly reduces the sintering time, and ensures a high heating rate, which ensures low entrainment of cesium into the gas phase [34–41].

The work aimed to obtain solid-state matrices by the SPS method based on NaY zeolite for reliable immobilization of cesium radionuclides. The novelty of study are: (i) the effect of hydrothermal synthesis temperature on the characteristics of NaY zeolite was studied for the first time; (ii) the mechanism of spark plasma sintering of aluminosilicate ceramics based on crystalline $CsAlSiO_4$ was studied in detail; (iii) it was confirmed that the obtained solid-state matrices fully comply with the requirements of GOST R 50926–96 and ISO 6961:1982 and can be used for reliable immobilization of cesium radionuclides.

2. Materials and methods

2.1. Chemicals

Sodium metasilicate (Na_2SiO_3•5 H_2O), aluminum sulfate ($Al_2(SO_4)_3$•18 H_2O) and sodium hydroxide (NaOH) were used NaY zeolite synthesis. Cesium chloride (CsCl) was dissolved for model solutions preparation in order to study sorption characteristics. All chemicals were purchased from Sigma-Aldrich, 99.9% purity without additional purification.

2.2. Preparation of NaY zeolite sorbents

The synthesis of NAY zeolite with the required SiO_2/Al_2O_3 ratio in the range of 8.5–10.5 consisted in hydrothermal crystallization of alumosilicates hydrogel of the $14Na_2O·Al_2O_3·10SiO_2.800\ H_2O$ chemical composition. The hydrogel was prepared by mixing an alkaline solution of aluminum sulfate with a solution of liquid glass. Solutions of 0.45 M $Al_2(SO_4)_3$•18 H_2O and 0.84 M Na_2SiO_3•5 H_2O in a volume ratio of 1:9 were droplet added to the aliquot of 10 ml distilled water. The resulting hydrogel was intensively stirred on a magnetic stirrer at room temperature for 30 min. Crystallization of the obtained hydrogel was carried out by hydrothermal method in a 250 ml reactor at temperatures of 110, 130, 150 and 180 °C with an exposure time of 6 h. The resulting zeolite precipitate was filtered, washed with distilled water and dried at 90 °C for 1 h.

2.3. Sorption saturation of NaY zeolite by Cs^+ ions

Zeolite powders in batches of 1.0 g were placed in flasks with 100 ml of CsCl solution containing Cs^+ 5.0 g/L ions and kept for 24 h on a shaker at room temperature until sorption equilibrium was reached. Further, the samples were filtered, washed with distilled water and dried at 100 °C until the moisture was completely removed. The sorption capacity of cesium ions was determined by atomic absorption spectrometry by their residual content in solution.

2.4. Batch sorption experiment

The study of NaY zeolite sorption properties was carried out under batch conditions of stable cesium isotopes from distilled water. Sorption isotherms were obtained using solutions with different CsCl concentrations at an initial pH of 6.0 ± 0.5. The initial concentration of cesium ions in model solutions was ranged from 0.05 to 20 mmol/L.

10.0 mg sorbent suspension was placed in an Eppendorf tube and 10

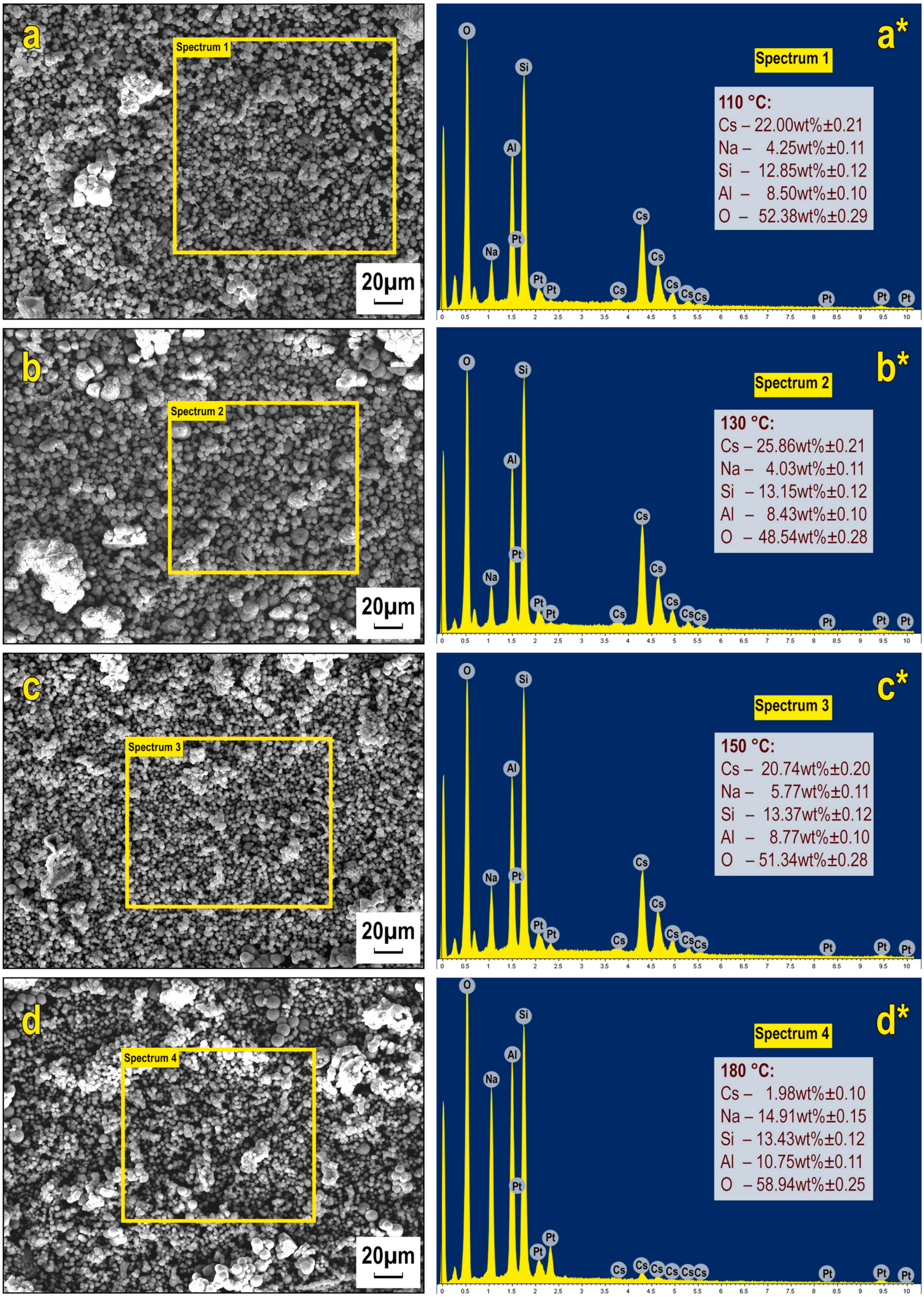

Fig. 2. SEM images and EDS distribution of elements in the structure of NaY-type zeolite samples at different synthesis temperatures (a, a*) - 110 °C, (b, b*) - 130 °C, (c, c*) - 150, (d, d*) - 180 °C.

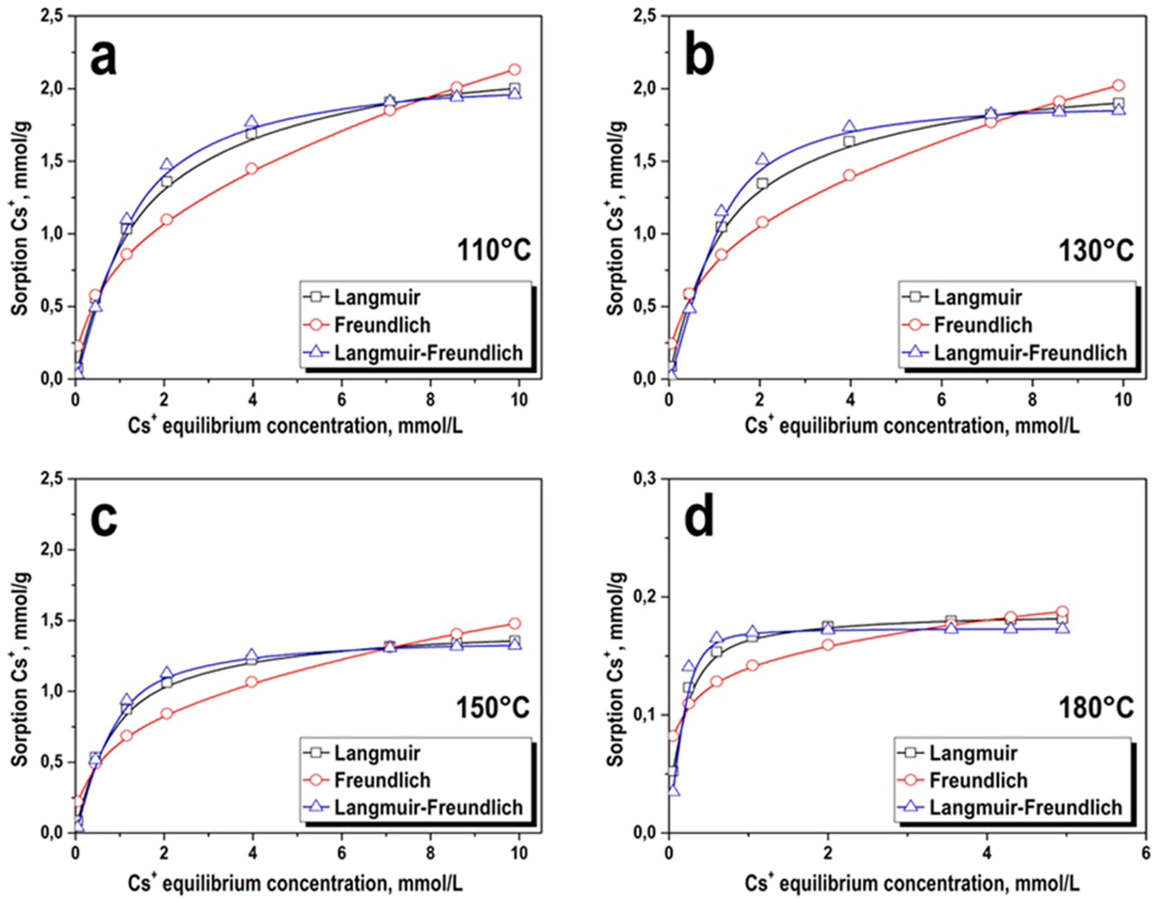

Fig. 3. Sorption isotherms of Cs+ ion on NaY zeolite samples.

Table 2
Calculated parameters of the Langmuir, Freundlich and Langmuir-Freundlich equations for Cs+ ions sorption.

Isotherm model	Parameters	NaY 110 °C	NaY 130 °C	NaY 150 °C	NaY 180 °C
Langmuir	G_{max} (mmol/g)	2.295 ± 0.087	2.129 ± 0.130	1.463 ± 0.089	0.186 ± 0.023
	K_L (L/g)	0.712 ± 0.092	0.835 ± 0.177	1.277 ± 0.293	7.808 ± 4.373
	R^2	0.99	0.98	0.98	0.85
Freundlich	$K_{F(}$ (mmol/g)× (L/mmol)n)	0.808 ± 0.129	0.808 ± 0.148	0.651 ± 0.10	0.140 ± 0.024
	m	0.422 ± 0.081	0.399 ± 0.094	0.357 ± 0.0803	0.179 ± 0.114
	R^2	0.94	0.91	0.90	0.52
Langmuir-Freundlich	G_{max} (mmol/g)	2.046 ± 0.030	1.885 ± 0.062	1.355 ± 0.089	0.172 ± 0.021
	K_{LF} (L/g)	0.949 ± 0.051	0.776 ± 0.181	1.833 ± 0.641	1.763 ± 0.573
	R^2	0.99	0.99	0.99	0.90

ml of model solution was poured (S:L = 1:1000 g/L). A series of test tubes was fixed on a vertical shaker and mixed at a rate of 20 rpm for 48 h. After that, the sorbent was separated from the solution on the "blue ribbon" filter and the residual content of Cs^+ ions was determined by atomic absorption spectrometry.

For mathematical processing of experimental data of sorption isotherms, well-known sorption models at the S/L boundary were used. The sorption capacity (q_e) was calculation according to Eq. (1):

$$q_e = \frac{(C_0 - Ce)\bullet VV}{m \times 100\%} \quad (1)$$

where q_e is the sorption capacity (wt%), C_0 is the initial concentration of Cs^+ ions before adsorption (g L^{-1}), C_e is the final concentration of Cs^+ ions after adsorption (g L^{-1}), V is the volume of Cs^+ ion solution (L), and m is the absorber mass supplied (g).

Freundlich equation:

$$G = K_F \bullet C^m, \quad (2)$$

where C is the equilibrium concentration of Cs^+ ions (mg/L); K_F is the Freundlich constant, which characterizes the relative adsorption capacity and represents the value of adsorption at an equilibrium concentration equal to one; m is an indicator of the heterogeneity of exchange centers, which characterizes the change in the adsorption energy depending on the degree of their filling.

Langmuir equation:

$$\frac{G \ = G_{max} K_L \bullet CC}{1 + K_L \bullet CC} \quad (3)$$

where G_{max} is maximum sorption capacity (mg/g); C is the equilibrium concentration of Cs^+ ions (mg/L); K_L is Langmuir adsorption equilibrium constants characterizing the adsorbent-adsorbate interaction.

Langmuir-Freundlich equation:

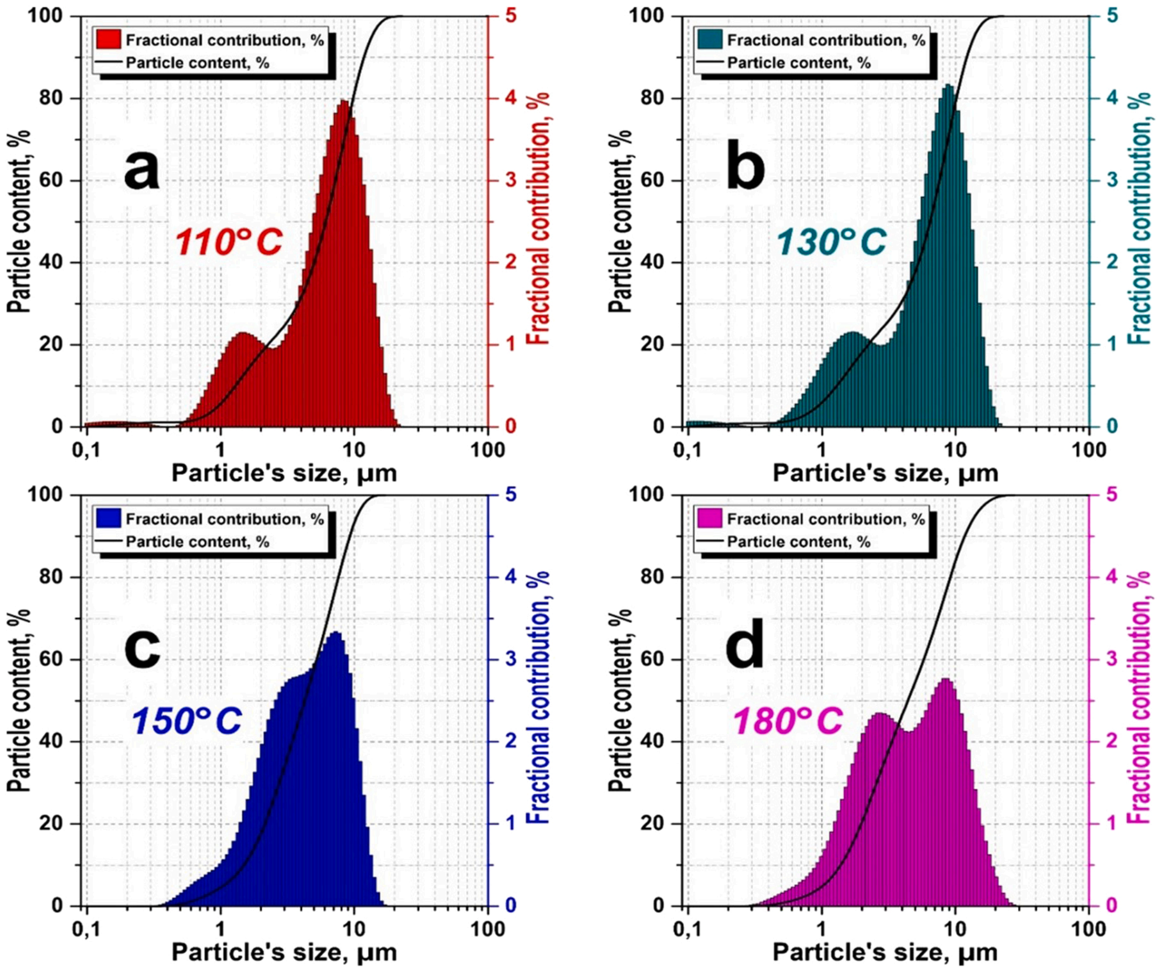

Fig. 4. Distribution of particle size of NaY zeolites obtained at (a, a*) 110, (b, b*) 130, (c, c*) 150 and (d, d*) 180 °C.

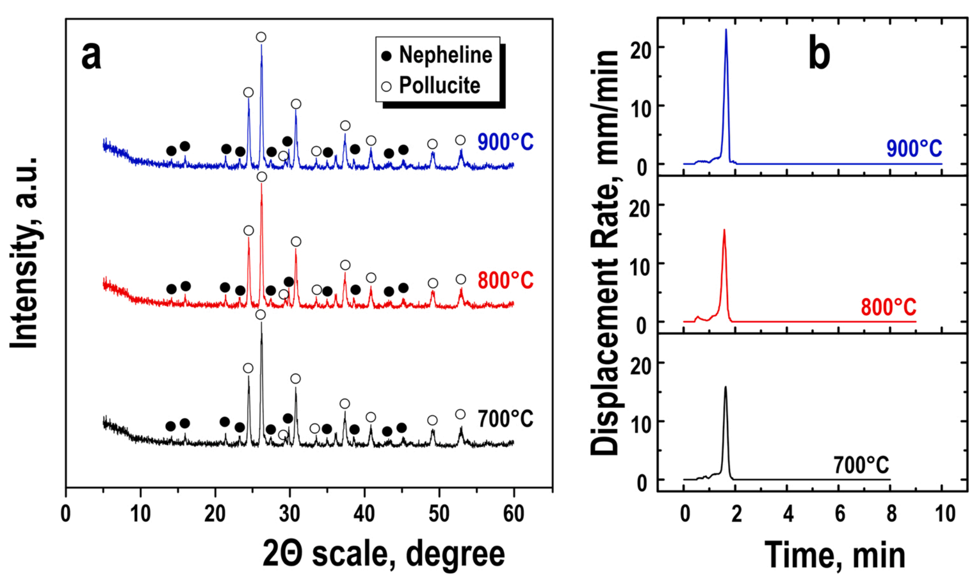

Fig. 5. (a) XRD patterns and (b) dilatometry curves of solid-state matrices prepared by SPS.

$$G = \frac{G_{max} K_{LF} \bullet C^m}{1 + K_{LF} \bullet C^m}, \quad (4)$$

where G_{max} is maximum sorption capacity (mg/g); C is the equilibrium concentration of Cs^+ ions (mg/L); K_{LF} is Langmuir-Freundlich adsorption equilibrium constant; m is an indicator of the heterogeneity of exchange centers. The approximation of experimental data by the specified equations in a nonlinear form was carried out using the "SciDAVis" program.

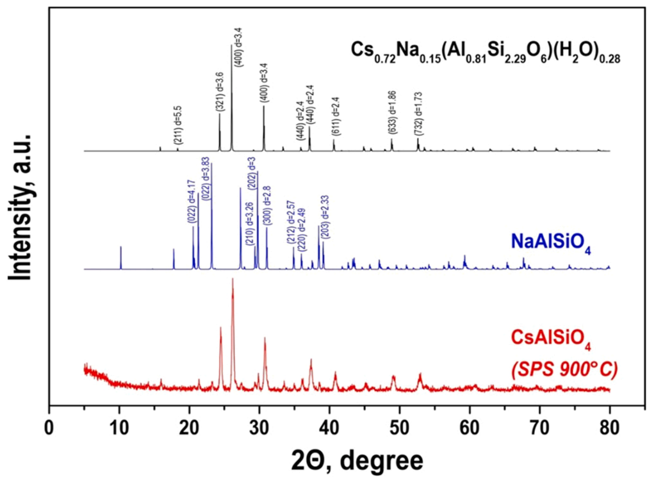

Fig. 6. XRD patterns of the sample obtained by SPS at 900 °C and the individual crystalline phases of Cs0.72Na0.15Al0.81Si2.19O6·0.28H2O and NaAlSiO4.

2.5. Spark plasma sintering of NaY samples

The synthesis of ceramic matrices was carried out by the method of spark plasma sintering of powders on the SPS-515S installation of the "Dr. Sinter·LAB TM" company (Japan). Zeolite powder of 1.0 g was placed in a graphite mold (working diameter 10 mm), pressed at a pressure of 20.7 MPa, then the sample was placed in a vacuum chamber (residual pressure 6.0 Pa) and sintered. The sample was heated by a constant electric current with a forced supply of periodic low-voltage pulses in the On/Off mode with a frequency of 12/2, a pulse packet duration of 39.6 ms and a pause of 6.6 ms. The sintering temperatures were 700, 800 and 900 °C, the heating rate was regulated in stages: 300 °C/min in the temperature range from 20° to 650°C, then from 650 °C and above - 90 °C/min. The samples were kept at the final temperature for 5 min with further cooling for 30 min to room temperature. The formation pressure was constant and amounted to 57.3 MPa.

2.6. Analytical methods

The crystal phases of the samples were identified using X-ray phase analysis (XRD) with CuKα-radiation, Ni-filter, average wavelength (λ) 1.5418 Å, shooting angle range 2θ 10–80°, scanning step 0.02°, registration rate of spectra - 5°/min on a diffractometer "D8 Advance Bruker AXS" (Germany).

The thermogravimetric curves were recorded on the DTG-60 H Shimadzu device in platinum crucibles with a pierced lid in a dry argon stream (20 ml/min) in the temperature range of 35–1300 °C and the heating rate of 10 °C/min. Particle size distribution was determined on a particle size analyzer Analysette-22 NanoTec/MicroTec/XT Fritsch (Germany). The structure of the studied materials was evaluated by scanning electron microscopy (SEM) on the CrossBeam 1540 XB "Carl Zeiss" device (Germany). The appearance density ($\rho_{app.}$) was measured by hydrostatic weighing on the scales of Adventurer TM "OHAUS Corporation" (USA). The concentration of cesium ions in solution was determined by atomic absorption spectrometry (AAS) on a SOLAAR M6 "Thermo" spectrometer (USA). The Vickers microhardness (HV) was measured at a load of HV0.5 on HMV-G-FA-D (Shimadzu, Japan). Compressive strength was evaluated on the Autograph AG-X plus 100kH tensile testing unit (Shimadzu, Japan) at a displacement rate of 0.5 mm/min.

2.7. Evaluation of Cs^+ ions leaching

The hydrolytic stability of ceramic matrices was evaluated by the rate of cesium ions leaching during prolonged contact with an aqueous medium at room temperature, according to GOST R 52126–2003. A solution of distilled water was used for the study. Determination of the concentration of desorbed cesium from the matrices into the solution was carried out on 1, 3, 5, 7, 14, 30 day, using the method of atomic absorption spectrometry. The experimental results were processed according to the Eq. (5):

$$R_i^n = \frac{m_n^i}{M_0^i \cdot S \cdot t_n},\ \mathrm{g} \Big/ \left(\mathrm{cm}^2 \cdot \mathrm{day}\right), \tag{5}$$

where m^i_n is the weight, g, of element i leached during the n-th test time interval t_n, day, M^i_0 is the weight content, g/g, of element i in the matrices, S is the geometric surface area of the sample, cm^2.

The effective diffusion coefficient (D_e) was calculated by transformations of Fick's second law (Eq. 6) according to the methodology described in [42]:

$$\frac{\sum m}{M_0} = 2\left(\frac{D_e}{\pi}\right)^{\frac{1}{2}}\left(\frac{S}{V}\right)t^{\frac{1}{2}} + \alpha, \tag{6}$$

Table 3
Physico-mechanical characteristics of matrices obtained by SPS.

Sample	Temperature of sinthering, °C	$\rho_{app.}$, g/cm^3	R, g/cm^2·day	σ_{comp}, MPa	HV
NaY zeolite 110 °C	700	2.23	$3.5 \cdot 10^{-5}$	53. 4	90
	800	2.63	$1.1 \cdot 10^{-5}$	89.7	104
	900	2.72	$2.3 \cdot 10^{-8}$	132.9	619

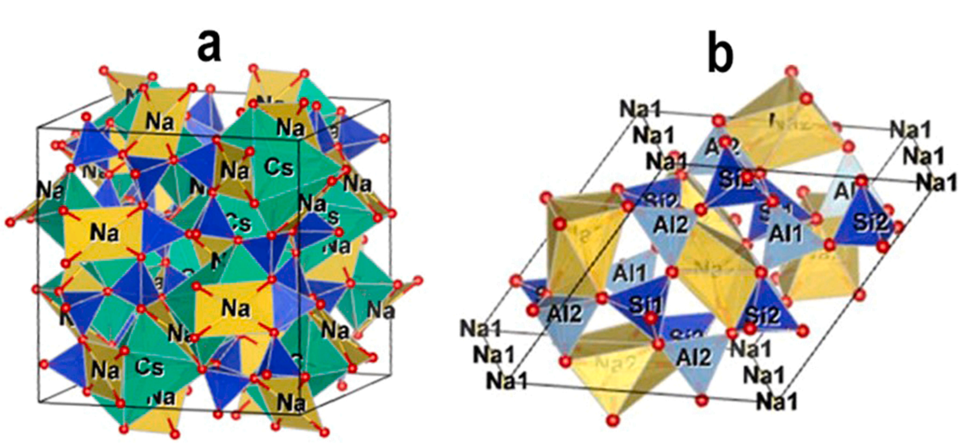

Fig. 7. Model image of (a) $Cs_{0.72}Na_{0.15}Al_{0.81}Si_{2.19}O_6 \cdot 0.28\ H_2O$ and (b) $NaAlSiO_4$ crystal structure.

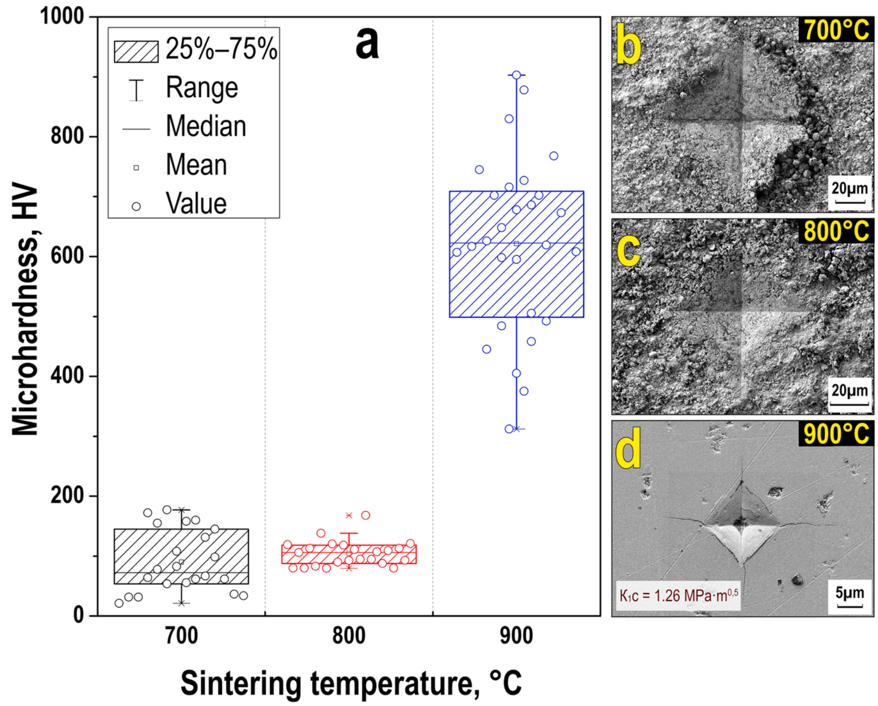

Fig. 8. Dispersion of Vickers microhardness of NaY zeolite ceramic samples synthesized by SPS at different temperatures and SEM images Vickers index fingerprints.

where *m* is the cesium weight, mg, leached over a time interval *t*, s, M_0 is the initial cesium content in the sample, mg, D_e is the effective diffusion coefficient, cm^2/s, *S* is the surface area of the sample, cm^2, *V* is the volume of the sample, cm^3, *α* is a parameter that takes into account the weight of leached cesium at the initial sample contact with distilled water.

This equation was reduced to a linear form by introducing the coefficient *K* (Eq. 7), which is the tangent of the slope angle of the direct dependence of the cesium fraction leached from the sample on the square root of the contact time of the material with the leaching solution:

$$K = 2\left(\frac{D_e}{\pi}\right)^{0,5} \bullet \left(\left(\frac{S}{V}\right),\right. \quad (7)$$

The effective diffusion coefficient was calculated according to Eq. (8):

$$D_e = \frac{K^2 \bullet \pi\pi}{4 \bullet \left(\frac{V}{S}\right)^2} \quad (8)$$

The leaching index *L* was calculated as the decimal logarithm of the inverse diffusion value [43]:

$$L = \lg\frac{1}{D_e} \quad (9)$$

Estimation of the dominant leaching mechanism based on the dependence of the decimal logarithm of the accumulated fraction of leached radionuclide (B_t, mg/m^2) on the decimal logarithm of the leaching time *t*, s by Eq. (10):

$$lg \quad (B_t) = \frac{1}{2}\lg t + lg\left[U_{max} d\sqrt{\frac{D_e}{\pi}}\right] \quad (10)$$

Where U_{max} is maximum amount of leached radionuclide, mg/kg, *d* is density of matrices, kg/m^3.

The leaching depth of the matrices characterizes the matrices destruction during contact with an aqueous solution and was calculated by Eq. (11):

$$L_t^i = \sum\nolimits_1^n \left(W_n^i \cdot \frac{t_n}{d}\right) \quad (11)$$

where L_t^i is leaching depth of the matrices reached during interval time t_n, cm, *d* is density of matrices, kg/m^3.

3. Results and discussions

According to the XRD results (Fig. 1a), it was found that the NAY zeolite of the Fojasite structure was obtained during hydrothermal treatment of alumosilicates hydrogel at 110–150 °C. At a higher temperature, sodium aluminosilicate hydrate $Na_2Al_2Si_{2.4}O_{8.8}$·6.7 H_2O was formed.

The thermal stability of a cesium-saturated NaY zeolite was studied during calcination up to 1300 °C in air. According to the DTA-TGA data (Fig. 1b), heating of the sample to 500 °C was accompanied by an endothermic effect and a mass loss of 11.6 wt% due to the removal of physically and chemically bound water. In the temperature range of 1000–1100 °C, the presence of an exothermic effect was revealed, which indicated a phase transition and, accordingly, a change in the crystal structure. A decrease in mass above 960 °C may be associated with a slight entrainment of cesium into the gas phase. Based on the presented results, a sample obtained by hydrothermal treatment at 110 °C was selected for the synthesis of solid-state matrices.

The highest weight content of cesium ions (26.1 wt%) was achieved for samples obtained by hydrothermal treatment at 110 and 130 °C, characterized by similar specific surface area of 410 and 417 m^2/g, respectively (Table 1).

The calculation of sorption capacity was performed according to Eq. (1). Fig. 2 shows that with an increase in the temperature of the hydrothermal synthesis of NaY type zeolite the sorption capacity was changed. At temperatures of 110 and 130 °C the sorption capacity was increased, followed by an increase in temperature, the sorption capacity of cesium was decreased, which correlates with the data obtained by atomic adsorption.

According to the C. H. Giles classification [44], the sorption isotherms of cesium ions (Fig. 3a) could be attributed to the H-type, which

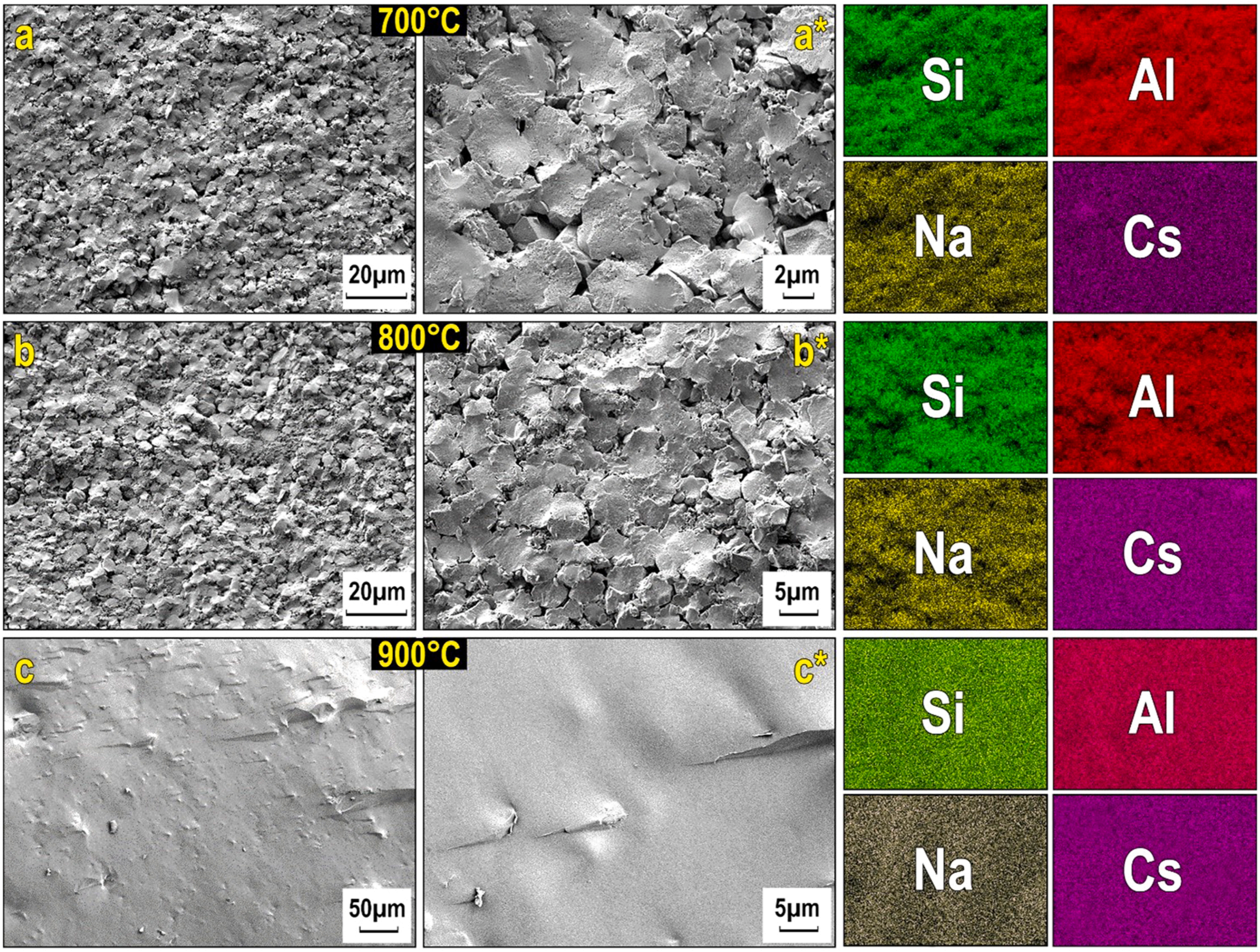

Fig. 9. SEM of solid-state matrices obtained by SPS at (a, a*) – 700, (b, b*) – 800, (c, c*) 900 °C.

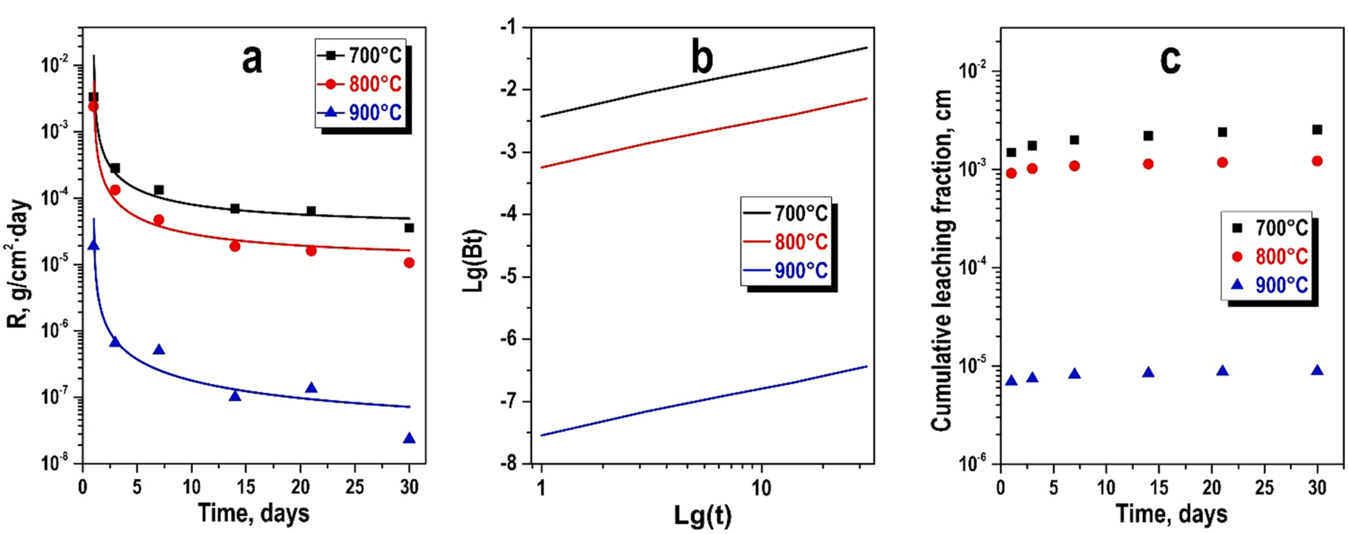

Fig. 10. Parameters of cesium leaching from $CsNaAlSiO_4$ matrices prepared by SPS at 700, 800, 900 °C: (a) rate of cesium leaching; (b) logarithmic dependences of the accumulated fraction of leached cesium on the leaching time; (c) – leaching depth.

is characterized by a vertical initial section, due to the high affinity of sorption sites to cesium ions. All isotherms were characterized by a well-defined plateau, which indicates the achievement of adsorption equilibrium and the filling of all sorption sites with adsorbate molecules. It was shown that with an increase in the temperature of hydrothermal synthesis, the sorption capacity decreased from 2.05 to 0.17 mmol/g,

Table 4
Parameters of cesium leaching from matrices obtained at different SPS temperatures.

Sintering temperature, °C	D_e, cm^2/s	L	U_{max}, mg/kg
700	$2.84{\bullet}10^{-8}$	7.55	$5.96{\bullet}10^{-2}$
800	$2.91{\bullet}10^{-9}$	8.54	$2.41{\bullet}10^{-2}$
900	$1.41{\bullet}10^{-13}$	12.85	$1.69{\bullet}10^{-4}$

Table 5
The comparison characteristics for solid-state matrices.

Parameter	According toGOST R 50926–96	Matrices prepared by SPS at 900 °C	Control method
Leaching rate of^{133}Cs, $g/cm^2{\cdot}day$	$< 10^{-5}$	$2.3{\cdot}10^{-8}$	GOST R 52126–2003 (ISO 6961:1982)
Comprehensive strength, MPa	> 9	132.9	Tests on a bursting machine
Thermal stability, °C	> 550	Up to 1300	XRD, DTA-TG
Uniformity of the structure in the volume of the glass block	Homogeneous	Homogeneous	XRD and SEM

which indicates a decrease in the number of sorption sites. Therefore, this may be due to a decrease in the specific surface area and the pore volume of the samples (Table 1), and consequently, the availability of ion exchange sites.

The decrease in sorption capacity may be due to an increase in the size and agglomeration of particles, as shown in the distribution of particle size for samples obtained in the range of 110–150 °C (Fig. 3a-c*). The sample obtained at 180 °C had the smallest sorption capacity of 0.17 mmol/g, characterized by the lowest value of BET specific surface area (Table 1). This indicates that the phase composition changes during hydrothermal synthesis of 180 °C (Fig. 1a) and the specific surface area decreases, which was accompanied by low sorption characteristics to Cs^+ ions.

Table 2 shows the calculated parameters for sorption models. Based on the high values of the correlation coefficients (R^2) and the correspondence of the calculated and experimental values of the sorption capacity. Thus, the experimental data were reliably described by the Langmuir-Freundlich equation. This indicates the occurrence of predominantly monomolecular adsorption at the initial stage, which is characteristic of the ion exchange sorption mechanism. The sample obtained at 110 °C had the highest sorption capacity, which is probably due to its chemical composition (Fig. 1) and the largest number of active ion exchange sites on the surface of NaY zeolite.(Fig. 4).

The sintering of cesium-saturated zeolite was carried out under conditions of spark plasma sintering at temperatures of 700, 800 and 900 °C. According to XRD data (Fig. 5a) the formation of nepheline ($NaAlSiO_4$) and pollucite ($Cs_{0.72}Na_{0.15}Al_{0.81}Si_{2.19}O_6{\cdot}0.28\ H_2O$) occurred at 700–900 °C. Herein, the highest shrinkage rate of solid-state matrices was established for SPS at 900 °C (Fig. 5b).

For a more detailed analysis of the crystal structure and phase composition of the ceramic matrices, Fig. 6 presents comparative XRD patterns of the sample obtained by SPS at 900 °C and the individual crystalline phases of $Cs_{0.72}Na_{0.15}Al_{0.81}Si_{2.19}O_6{\cdot}0.28\ H_2O$ and $NaAlSiO_4$.

In order to visualize the crystal structures of the obtained ceramics, structural 3D models were constructed (Fig. 7) using VESTA software. A comparative analysis of the experimental X-ray of the ceramics obtained at 900 °C and the X-ray of nepheline and pollucite constructed on the CAD database was carried out.

The main characteristics of the matrices are presented in Table 3. Thus, with an increase in the sintering temperature from 700° to 900°C, an increase in apparent density (2.23–2.72 g/cm^3), mechanical compressive strength (53.4–132.9 MPa) and Vickers microhardness (100−900) was observed.

To analyze the microhardness, a value span diagram was used, which is an indirect assessment of the strength microhardness of the material (Fig. 8). According to obtained data, with an increase in the sintering temperature, the hardness of ceramic materials increased from 100 to 900 HV. This was primarily due to consolidation efficiency of sintered powder into a denser compact, as well as grain growth and the formation of dense ceramics.

This indicates an increase in the density of samples during sintering and is in good agreement with the results of dilatometric studies (Fig. 5b). Also, the lowest cesium leaching R ($2.3{\cdot}10^{-8}$ $g/cm^2{\cdot}day$) was achieved for the sample obtained by SPS at 900 °C.

According to the results of the SEM, it was found that the surface structure of all samples has similar features. SPS consolidation was accompanied by dense packing and active sintering of zeolite particles. At temperatures of 700 and 800 °C, the powder particles were significantly deformed during sintering, partially preserving the contour of the shape and the contact boundaries (Fig. 9). At a temperature of 900 °C, the particles were completely sintered into a monolithic structure. In addition, the surface of the samples had large defects and small pores (Fig. 9a, a*, b, b*). The size of the defects and the number of pores were reduced by increasing the sintering temperature up to 900 °C.

The highest density of the structure was characteristic of the sample after the SPS process at 900 °C, which is consistent with the dilatometric dependencies shown in Fig. 9a. Based on the results of the powder compaction dynamics, it was found that the activation of solid-phase sintering processes of particles occurred at 2 min for synthesis at 600 °C. Slight compaction up to 600 °C was realized due to pressing.

The hydrolytic stability of the obtained matrices was evaluated, which is the main indicator of their effectiveness for cesium radionuclides immobilization. The lowest rate of cesium leaching was observed in samples obtained at 900 °C. This indicator reached $2.33{\cdot}10^{-8}$ g $/cm^2{\cdot}day$, which met the requirements of GOST R 50926–96 for high-level waste (Fig. 10a). The high hydrolytic stability of matrices was due to their chemical composition. The increase in this indicator for samples obtained at an elevated sintering temperature was due to a decrease in the defects number.

The value of the tangent of inclination angle for the straight lines related to the matrices obtained at 700 and 800 °C (Fig. 10b) was close to 0.5, which indicates the predominance of the diffusion leaching mechanism, according to the de Groot and van der Sloot model [28,29]. The tangent of the curve corresponding to sintering at 900 °C tended to 1, which means that the dissolution of the surface occurs earlier than the internal diffusion. Calculated indicators of the leaching depth are shown in Fig. 10c. Ceramic matrices had great stability in distilled water, due to the dense structure and chemical resistance.(Table 4).

A comparative analysis of the qualitative characteristics of the matrices studied in the work on the example of a sample obtained at 900 °C and the requirements of the regulatory document on cured radioactive waste showed that the sample has high quality indicators and meets regulatory requirements (Table 5).

4. Conclusions

Hydrothermal synthesis of NaY zeolite was successfully carried out at a temperature of 110–180 °C. An increase in temperature led to a slight increase in the dispersion of particles, the average size of which was 5–8 μm. The largest sorption capacity (26.1 wt%) for cesium was reached for a sample obtained at 110 °C, with a specific surface area of 409 m^2/g. The cesium-saturated NaY had thermal stability up to 1300 °C and a low transition of cesium to the gas phase. Solid-state matrices with pollucite and nepheline structures were obtained by spark plasma sintering at 700, 800 and 900 °C. The process of shrinkage and sintering of the powder at 700–900 °C proceeded in a short time

~2–3 min. With an increase in the sintering temperature, the density, mechanical strength and Vickers microhardness of ceramics increased significantly. The sample obtained at 900 °C had the highest hydrolytic stability (the cesium leaching rate $R_{Cs} \sim 10^{-8}$ g·cm^{-2} day^{-1}, the diffusion coefficient D_e ~1.41 ×10^{-13} cm^2/s), HV~ 698, Fracture toughness (K_{1c}) ~ 1.26 MPa m$^{1/2}$. The obtained matrices are suitable for reliable and safe immobilization of cesium radionuclides.

Declaration of Competing Interest

The authors declare that they have no known competing financial interests or personal relationships that could have appeared to influence the work reported in this paper.

Acknowledgments

The study was carried out with financial support from the State Assignment of the Ministry of Science and Higher Education of the Russian Federation, topic No. 00657-2020-0006, Yun Shi acknowledges the support by the Strategic Priority Research Program of the Chinese Academy of Sciences (XDA22010301).

References

[1] B. Alshuraiaan, S. Pushkin, A. Kurilova, M. Mazur, Management of the energy and economic potential of nuclear waste use, Energies 14 (2021) 3709, https://doi.org/10.3390/en14123709.
[2] J. Liu, W. Dai, Overview of nuclear waste treatment and management, in: E3S Web of Conferences, EDP Sciences, 2019, https://doi.org/10.1051/e3sconf/201911804037.
[3] N.K. Gupta, A. Sengupta, A. Gupta, J.R. Sonawane, H. Sahoo, Biosorption-an alternative method for nuclear waste management: a critical review, J. Environ. Chem. Eng. 6 (2018) 2159–2175, https://doi.org/10.1016/j.jece.2018.03.021.
[4] F. Diaz-Maurin, H.C. Sun, J. Yu, R.C. Ewing, Evolution and structure of the scientific basis for nuclear waste management, MRS Adv. Mater. Res. Soc. (2019) 959–964, https://doi.org/10.1557/adv.2018.636.
[5] Management of Spent Fuel from Nuclear Power Reactors Learning from the Past, Enabling the Future, IAEA, 2019.
[6] A.I. Ivanets, I.L. Shashkova, N.V. Kitikova, M.V. Maslova, N.V. Mudruk, New heterogeneous synthesis of mixed Ti-Ca-Mg phosphates as efficient sorbents of 137Cs, 90Sr and 60Co radionuclides, J. Taiwan Inst. Chem. Eng. 104 (2019) 151–159, https://doi.org/10.1016/j.jtice.2019.09.001.
[7] A.I. Ivanets, V. Srivastava, N.V. Kitikova, I.L. Shashkova, M. Sillanpää, Kinetic and thermodynamic studies of the Co(II) and Ni(II) ions removal from aqueous solutions by Ca-Mg phosphates, Chemosphere 171 (2017) 348–354, https://doi.org/10.1016/j.chemosphere.2016.12.062.
[8] Identification of Radioactive Sources and Devices, IAEA, 2007.
[9] K. v Martynov, A.N. Nekrasov, A.R. Kotel'nikov, I.G. Tananaev, Synthesis and study of the chemical stability and strength of zirconium phosphates with the structure of langbeinite with imitators of high-level radioactive waste (HLRW), Glass Phys. Chem. 43 (2017) 75–82, https://doi.org/10.1134/S1087659617010096.
[10] F. Wang, Y. Wang, Q. Liao, J. Zhang, W. Zhao, Y. Yuan, H. Zhu, L. Li, Y. Zhu, Immobilization of a simulated HLW in phosphate based glasses/glass-ceramics by melt-quenching process, J. Non Cryst. Solids 545 (2020), 120246, https://doi.org/10.1016/j.jnoncrysol.2020.120246.
[11] V.I. Pet'Kov, A.S. Shipilov, M. v Sukhanov, Thermal expansion of MZr2(AsO4)3 and MZr2(TO4) x (PO4)3-x (M = Li, Na, K, Rb, Cs; T = As, V), Inorg. Mater. 51 (2015) 1079–1085, https://doi.org/10.1134/S002016851510012X.
[12] R.A. Kuznetsov, I.G. Kanterman, V. v Eremin, V.G. Semenov, Ultradisperse composite vitrified host materials of monazite–iron (pyro)phosphate type for conservation of nuclear waste concentrates, Radiochemistry 60 (2018) 323–327, https://doi.org/10.1134/S1066362218030165.
[13] P. Tumurugoti, B.M. Clark, D.J. Edwards, J. Amoroso, S.K. Sundaram, Cesium incorporation in hollandite-rich multiphasic ceramic waste forms, J. Solid State Chem. 246 (2017) 107–112, https://doi.org/10.1016/j.jssc.2016.11.007.
[14] J. Zhao, J. Li, H. Liu, X. Zhang, K. Zheng, H. Yu, Q. Lian, H. Wang, Y. Zhu, J. Huo, Cesium immobilization in perovskite-type Ba1-x(La, Cs)xZrO3 ceramics by sol-gel method, Ceram. Int. 46 (2020) 9968–9971, https://doi.org/10.1016/j.ceramint.2019.12.219.
[15] B.M. Clark, P. Tumurugoti, S.K. Sundaram, J.W. Amoroso, J.C. Marra, Preparation and characterization of multiphase ceramic designer waste forms, Sci. Rep. 11 (2021) 4512, https://doi.org/10.1038/s41598-021-84014-1.
[16] J. Ma, Z. Fang, X. Yang, B. Wang, F. Luo, X. Zhao, X. Wang, Y. Yang, Investigating hollandite–perovskite composite ceramics as a potential waste form for immobilization of radioactive cesium and strontium, J. Mater. Sci. 56 (2021) 9644–9654, https://doi.org/10.1007/s10853-021-05886-2.
[17] M. Zhao, P. Russell, J. Amoroso, S. Misture, S. Utlak, T. Besmann, L. Shuller-Nickles, K.S. Brinkman, Exploring the links between crystal chemistry, cesium retention, thermochemistry and chemical durability in single-phase (Ba,Cs)1.33 (Fe,Ti)8O16 hollandite, J. Mater. Sci. 55 (2020) 6401–6416, https://doi.org/10.1007/s10853-020-04447-3.
[18] M. Zhao, J.W. Amoroso, K.M. Fenker, D.P. Diprete, S. Misture, S. Utlak, T. Besmann, K. Brinkman, The effect of cesium content on the thermodynamic stability and chemical durability of (Ba,Cs)1.33(Al,Ti)8O16 hollandite, Am. Ceram. Soc. 103 (2020) 7310–7321, https://doi.org/10.1111/jace.17422.
[19] A.I. Orlova, E.E. Loginova, A.A. Logacheva, V.T. Demarin, O. v Shmidt, A. Yu Nikolaev, A crystal-chemical approach in the development of phosphate materials as environmentally safe chemical forms of utilization of spent Cs-containing ferrocyanide sorbents, Radiochemistry 52 (2010) 462–468, https://doi.org/10.1134/s1066362210050024.
[20] M. Omerašević, M. Lukić, M. Savić-Biserčić, A. Savić, L. Matović, Z. Baščarević, D. Bučevac, Permanent disposal of Cs ions in the form of dense pollucite ceramics having low thermal expansion coefficient, Nucl. Eng. Technol. 52 (2020) 115–122, https://doi.org/10.1016/j.net.2019.07.001.
[21] T.A. Vereshchagina, S.N. Vereshchagin, N.N. Shishkina, N.G. Vasilieva, L. A. Solovyov, A.G. Anshits, Microsphere zeolite materials derived from coal fly ash cenospheres as precursors to mineral-like aluminosilicate hosts for 135,137Cs and 90Sr, J. Nucl. Mater. 437 (2013) 11–18, https://doi.org/10.1016/j.jnucmat.2013.01.343.
[22] A. Ivanets, I. Shashkova, N. Kitikova, A. Radkevich, E. Venhlinskaya, A. Dzikaya, A. V. Trukhanov, M. Sillanpää, Facile synthesis of calcium magnesium zirconium phosphate adsorbents transformed into MZr4P6O24 (M: Ca, Mg) ceramic matrix for radionuclides immobilization, Sep. Purif. Technol. 272 (2021), 118912, https://doi.org/10.1016/j.seppur.2021.118912.
[23] S. Kwon, C. Kim, E. Han, H. Lee, H.S. Cho, M. Choi, Relationship between zeolite structure and capture capability for radioactive cesium and strontium, J. Hazard. Mater. 408 (2021), 124419, https://doi.org/10.1016/j.jhazmat.2020.124419.
[24] M. Luo, M. Wen, J. Wang, J. Zhu, The study of cooperation solidification of Cs based on ZSM-5 zeolite, in: Energy Procedia, Elsevier Ltd, 2013, pp. 434–442, https://doi.org/10.1016/j.egypro.2013.07.234.
[25] L.J. Gardner, S.A. Walling, C.L. Corkhill, N.C. Hyatt, Thermal treatment of Cs-exchanged chabazite by hot isostatic pressing to support decommissioning of Fukushima Daiichi Nuclear Power Plant, J. Hazard. Mater. 413 (2021), 125250, https://doi.org/10.1016/j.jhazmat.2021.125250.
[26] Y. Yang, T. Wang, Z. Zhang, Z. Ke, C. Shan, X. Cao, L. Ma, S. Peng, A novel method to convert Cs-polluted soil into pollucite-base glass-ceramics for Cs immobilization, Chem. Eng. J. 385 (2020), 123844, https://doi.org/10.1016/j.cej.2019.123844.
[27] M. Omerašević, J. Ružić, B.N. Vasiljević, Z. Baščarević, D. Bučevac, J. Orlić, L. Matović, Transformation of Cs-exchanged clinoptilolite to CsAlSi5O12 by hot-pressing, Ceram. Int. 43 (2017) 13500–13504, https://doi.org/10.1016/j.ceramint.2017.07.055.
[28] S. Chen, J.F. Guo, B. Xu, X.W. Sun, Sintering of Metakaolin-based Na-Pollucite ceramics and their immobilization of Cs, Ann. Nucl. Energy 145 (2020), 107595, https://doi.org/10.1016/j.anucene.2020.107595.
[29] M. Omerašević, L. Matović, J. Ružić, Ž. Golubović, U. Jovanović, S. Mentus, V. Dondur, Safe trapping of cesium into pollucite structure by hot-pressing method, J. Nucl. Mater. 474 (2016) 35–44, https://doi.org/10.1016/j.jnucmat.2016.03.006.
[30] L.C. Harnett, L.J. Gardner, S.K. Sun, C. Mann, N.C. Hyatt, Reactive spark plasma sintering of Cs-exchanged chabazite: characterisation and durability assessment for Fukushima Daiichi NPP clean-up, J. Nucl. Sci. Technol. 56 (2019) 891–901, https://doi.org/10.1080/00223131.2019.1602484.
[31] A.I. Orlova, M.I. Ojovan, Ceramic mineral waste-forms for nuclear waste immobilization, Materials 12 (2019), https://doi.org/10.3390/ma12162638.
[32] P. He, S. Fu, M. Wang, X. Duan, Q. Wang, D. Li, Z. Yang, D. Jia, Y. Zhou, B2O3-assisted low-temperature crystallization of pollucite structures and their potential applications in Cs+ immobilization, J. Nucl. Mater. 540 (2020), 152314, https://doi.org/10.1016/j.jnucmat.2020.152314.
[33] M. Omerašević, M. Lukić, M. Savić-Biserčić, A. Savić, L. Matović, Z. Baščarević, D. Bučevac, Permanent disposal of Cs ions in the form of dense pollucite ceramics having low thermal expansion coefficient, Nucl. Eng. Technol. 52 (2020) 115–122, https://doi.org/10.1016/j.net.2019.07.001.
[34] E.K. Papynov, O.O. Shichalin, V.Yu Mayorov, V.G. Kuryavyi, T.A. Kaidalova, L. V. Teplukhina, A.S. Portnyagin, A.B. Slobodyuk, A.A. Belov, I.G. Tananaev, V. A. Avramenko, V.I. Sergienko, SPS technique for ionizing radiation source fabrication based on dense cesium-containing core, J. Hazard. Mater. 369 (2019) 25–30, https://doi.org/10.1016/j.jhazmat.2019.02.016.
[35] O.O. Shichalin, E.K. Papynov, V.Yu Maiorov, A.A. Belov, E.B. Modin, I. Yu Buravlev, Yu.A. Azarova, A. v Golub, E.A. Gridasova, A.E. Sukhorada, I. G. Tananaev, V.A. Avramenko, Spark plasma sintering of aluminosilicate ceramic matrices for immobilization of cesium radionuclides, Radiochemistry 61 (2019) 185–191, https://doi.org/10.1134/S1066362219020097.
[36] E.K. Papynov, O.O. Shichalin, V.Yu Mayorov, E.B. Modin, A.S. Portnyagin, I. A. Tkachenko, A.A. Belov, E.A. Gridasova, I.G. Tananaev, V.A. Avramenko, Spark Plasma Sintering as a high-tech approach in a new generation of synthesis of nanostructured functional ceramics, Nanotechnol. Russ. 12 (2017) 49–61, https://doi.org/10.1134/S1995078017010086.
[37] E.K. Papynov, O.O. Shichalin, A.Yu Mironenko, A. v Ryakov, I. v Manakov, P. v Makhrov, I.Yu Buravlev, I.G. Tananaev, V.A. Avramenko, V.I. Sergienko, Synthesis of high-density pellets of uranium dioxide by spark plasma sintering in dies of different types, Radiochemistry 60 (2018) 362–370, https://doi.org/10.1134/S1066362218040045.
[38] E.K. Papynov, O.O. Shichalin, M.A. Medkov, D.N. Grishchenko, I.A. Tkachenko, A. N. Fedorets, V.S. Pechnikov, A. v Golub, I.Yu Buravlev, I.G. Tananaev, V.

A. Avramenko, Spark plasma sintering of special-purpose functional ceramics based on UO2, ZrO2, Fe3O4/α-Fe2O3, Glass Phys. Chem. 44 (2018) 632–640, https://doi.org/10.1134/S1087659618060159.

[39] Z.Y. Hu, Z.H. Zhang, X.W. Cheng, F.C. Wang, Y.F. Zhang, S.L. Li, A review of multi-physical fields induced phenomena and effects in spark plasma sintering: fundamentals and applications, Mater. Des. 191 (2020), 108662, https://doi.org/10.1016/j.matdes.2020.108662.

[40] S.B. Yarusova, O.O. Shichalin, A.A. Belov, S.A. Azon, I.Y. Buravlev, A.V. Golub, V. Y. Mayorov, A.V. Gerasimenko, E.K. Papynov, A.I. Ivanets, A.A. Buravleva, E. B. Merkulov, V.A. Nepomnyushchaya, O.V. Kapustina, P.S. Gordienko, Synthesis of amorphous KAlSi3O8 for cesium radionuclide immobilization into solid matrices using spark plasma sintering technique, Ceram. Int. 48 (2022) 3808–3817, https://doi.org/10.1016/j.ceramint.2021.10.164.

[41] E.K. Papynov, O.O. Shichalin, A.A. Belov, I.Yu Buravlev, A.S. Portnyagin, S. A. Azon, D.Kh Shlyk, A.A. Buravleva, Yu.A. Parot'kina, V.A. Nepomnyushchaya, Z. E. Kornakova, A. v Gridasov, I.G. Tananaev, V.I. Sergienko, Synthesis of mineral-like SrWO4 ceramics with the scheelite structure and a radioisotope product based on it, Russ. J. Inorg. Chem. 66 (2021) 1434–1446, https://doi.org/10.1134/S0036023621090114.

[42] P. Szajerski, A. Bogobowicz, A. Gasiorowski, Cesium retention and release from sulfur polymer concrete matrix under normal and accidental conditions, J. Hazard. Mater. 381 (2020), 121180, https://doi.org/10.1016/j.jhazmat.2019.121180.

[43] P. He, S. Fu, M. Wang, X. Duan, Q. Wang, D. Li, Z. Yang, D. Jia, Y. Zhou, B2O3-assisted low-temperature crystallization of pollucite structures and their potential applications in Cs+ immobilization, J. Nucl. Mater. 540 (2020), 152314, https://doi.org/10.1016/j.jnucmat.2020.152314.

[44] B.C. H. Giles, T.H. Macewan, S.N. Nakhwa, D. Smith, Solution Adsorption Isotherms, and its Use in Diagnosis of Adsorption Mechanisms and in Measurement of Specific Surface Areas of Solids, 1922.